

OPEN ACCESS

Rechargeable Manganese Dioxide||Hard Carbon Lithium Batteries in an Ether Electrolyte

To cite this article: Dawei Xia et al 2024 J. Electrochem. Soc. 171 030528

View the article online for updates and enhancements.

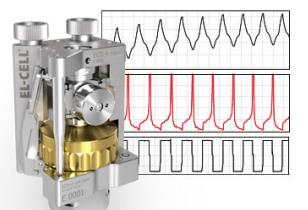
You may also like

- Molecular Structure Evaluation and Image-Guided Atomistic Representation of Hard Carbon Electrodes
- Jiaqi Li, Tianshuang Li, Chen Peng et al.
- 2023 roadmap for potassium-ion batteries
 Yang Xu, Magda Titirici, Jingwei Chen et al
- <u>Structure and function of hard carbon</u> <u>negative electrodes for sodium-ion</u> <u>batteries</u>

Uttam Mittal, Lisa Djuandhi, Neeraj Sharma et al.

Measure the Electrode Expansion in the Nanometer Range.

Discover the new ECD-4-nano!



- Battery Test Cell for Dilatometric Analysis (Expansion of Electrodes)
- Capacitive Displacement Sensor (Range 250 µm, Resolution ≤ 5 nm)
- Detect Thickness Changes of the Individual Electrode or the Full Cell.

www.el-cell.com +49 40 79012-734 sales@el-cell.com









Rechargeable Manganese Dioxide||Hard Carbon Lithium Batteries in an Ether Electrolyte

Dawei Xia,^{1,*} © Keith Rosenberg,¹ Yilin Li,² Anyang Hu,¹ Chengjun Sun,³ Luxi Li,³ Dennis Nordlund,⁴ Sami Sainio,⁴ Haibo Huang,² and Feng Lin^{1,5,6,*,z} ©

Earth-abundant, cost-effective electrode materials are essential for sustainable rechargeable batteries and global decarbonization. Manganese dioxide (MnO₂) and hard carbon both exhibit high structural and chemical tunability, making them excellent electrode candidates for batteries. Herein, we elucidate the impact of electrolytes on the cycling performance of commercial electrolytic manganese dioxide in Li chemistry. We leverage synchrotron X-ray analysis to discern the chemical state and local structural characteristics of Mn during cycling, as well as to quantify the Mn deposition on the counter electrode. By using an ether-based electrolyte instead of conventional carbonate electrolytes, we circumvent the formation of a surface Mn(II)-layer and Mn dissolution from Li_xMnO₂. Consequently, we achieved an impressive \sim 100% capacity retention for MnO₂ after 300 cycles at C/3. To create a lithium metal-lean full cell, we introduce hard carbon as the anode which is compatible with ether-based electrolytes. Commercial hard carbon delivers a specific capacity of \sim 230 mAh g⁻¹ at 0.1 A g⁻¹ without plateau, indicating a surface-adsorption mechanism. The resulting manganese dioxidellhard carbon full cell exhibits stable cycling and high Coulombic efficiency. Our research provides a promising solution to develop cost-effective, scalable, and safe energy storage solutions using widely available manganese oxide and hard carbon materials.

© 2024 The Author(s). Published on behalf of The Electrochemical Society by IOP Publishing Limited. This is an open access article distributed under the terms of the Creative Commons Attribution 4.0 License (CC BY, http://creativecommons.org/licenses/by/4.0/), which permits unrestricted reuse of the work in any medium, provided the original work is properly cited. [DOI: 10.1149/1945-7111/ad3415]

Manuscript submitted December 22, 2023; revised manuscript received February 23, 2024. Published March 27, 2024.

Supplementary material for this article is available online

Achieving global decarbonization encompasses the electrification of vehicles and infrastructures with sustainable energy storage systems. Lithium-ion batteries (LIBs) have garnered significant attention due to their exceptional advantages as an energy storage technology, including high energy density and excellent energy efficiency. The inclusion of elements such as cobalt (Co) and nickel (Ni) prevails in contemporary LIBs, which creates supply chain vulnerability due to their scarcity in the Earth's crust as well as high and fluctuating costs.² Beyond the rational selection of redox-active transition metals, other essential factors, such as manufacturing methods and scalability, need to be considered. Therefore, it is imperative to develop rechargeable batteries with Earth-abundant, scalable, and low-cost electrode materials that can be manufactured at low cost.^{3,4} Manganese-based oxide materials are particularly attractive due to their wide availability and versatility in forming various crystal structures, including spinel, layered, disordered rocksalt, and tunnel structures. 5.6 Many manganese-based oxide materials have shown promising properties across different battery systems, including non-aqueous and aqueous chemistries.

Manganese dioxide (MnO₂) has a long history of development and commercialization in energy storage and conversion. For example, electrolytic manganese dioxide (EMD) was commercialized in the 1970s as a cathode material for primary lithium batteries. ^{6,7} Micron-sized EMD has high volumetric energy density, enabling the popularity of compact primary Li-MnO₂ batteries in electronics. Chemical manganese dioxide (CMD), another category of MnO₂, is also widely studied because of its excellent structural and chemical tunability. Notable examples include γ -MnO₂ and α -MnO₂, which are composed of interconnected [MnO₆] octahedra yielding one-dimensional 1 \times 1 and 2 \times 2 tunnels, respectively. ^{8,9}

The tunnel structure can potentially enable reversible ion insertion/ extraction, yet long-term cyclable MnO₂ is rarely reported. Conventionally, the Li-MnO₂ primary battery is not believed to

Conventionally, the Li-MnO₂ primary battery is not believed to be rechargeable, even though manganese dioxide exhibits commendable structural reversibility. ^{10–12} One of the bottlenecks is the poor reversibility and the safety concerns of the lithium metal anode. Another concern is the Mn dissolution, migration, and deposition, which has been widely reported for Mn-rich materials. ^{13,14} If the dissolution could be eliminated, the cyclability of MnO₂ would be greatly enhanced in a rechargeable fashion. Mn(III) is present in the discharged MnO₂. Acidic species in the electrolyte can attack Mn (III) and trigger Mn dissolution. Therefore, electrolyte innovations become crucial to mitigate Mn dissolution to support the long cycle life of MnO₂-based rechargeable batteries without compromising their low-cost features. ¹⁵ Ether-based electrolytes using lithium imide salts are free of acid and thus become promising candidates to prolong the cyclability of MnO₂. ¹⁶ However, the structural and chemical state of cycled MnO₂ is underexplored, especially the impacts of different electrolytes on the surface Mn in a lithiated state.

To make viable MnO₂-based rechargeable LIBs, we need to have knowledge beyond the rational selection of electrolytes and an understanding of structural and chemical changes of cycled MnO₂ from the surface to bulk. Answering the following question also becomes critical: how can the MnO₂ cathode be effectively paired with a low-cost and scalable anode to maximize the cost benefit of MnO₂? Ether electrolytes are well known to be incompatible with graphite anode. In contrast, hard carbon can be an alternative. ^{17,18} Hard carbon is highly tunable and widely available, which can be advantageous in large-scale energy storage. In Na-ion batteries, hard carbon receives extensive attention. When cycled in ether electrolytes, hard carbon anodes exhibit higher initial Coulombic efficiency (ICE) and higher capacity than cycled in carbonate electrolytes. ¹⁹ To date, limited efforts are placed on the influences of electrolytes on hard carbon in LIBs.

¹Department of Chemistry, Virginia Tech, Virginia, 24061, United States of America

²Department of Food Science and Technology, Virginia Tech, Virginia, 24061, United States of America

³X-ray Science Division, Argonne National Laboratory, Lemont, Illinois, 60439, United States of America

⁴Stanford Synchrotron Radiation Lightsource, SLAC National Accelerator Laboratory, Menlo Park, California, 94025, United States of America

⁵Department of Materials Science and Engineering, Virginia Tech, Virginia, 24061, United States of America

⁶Macromolecules Innovation Institute, Virginia Tech, Virginia, 24061, United States of America

^{*}Electrochemical Society Member.

zE-mail: fenglin@vt.edu

Here, we systematically investigate the stability of MnO₂ upon repeated Li-ion storage in different electrolytes. We conclude that an ether-based electrolyte 1 M lithium bis(trifluoromethanesulfonyl) imide (LiTFSI) 1,3-Dioxane (DOL)/1,2-Dimethoxyethane (DME) can substantially mitigate Mn dissolution in Mn-based cathodes. The Mn chemical states at the surface and in the bulk are elucidated by synchrotron X-ray analysis. Commercial carbonate electrolytes lead to a Mn(II)-rich surface layer because of the disproportionation reaction of unstable Mn(III). In contrast, micron-sized EMD exhibits outstanding structural reversibility in 1 M LiTFSI DOL/DME even in the presence of abundant Mn³⁺, achieving approximately 100% capacity retention after 300 cycles at C/3. We then study the electrochemical behavior of a disordered carbon (hard carbon) anode in the ether electrolyte, aiming to establish a rechargeable hard carbon-MnO2 battery cell. The adsorption-based mechanism provides a capacity of \sim 230 mAh g⁻¹ for the hard carbon anode. To provide the initial Li inventory and compensate for the considerable lithium loss in the full cell during the first cycle, we introduce a thin Li metal layer on the hard carbon anode. Fluorescence X-ray microscopy further quantified the amount of Mn deposited on the hard carbon anode in the ether and carbonate electrolytes, providing strong evidence for the advantage of LiTFSI DOL/DME in inhibiting Mn dissolution. Our work provides a proof-of-concept design for applying MnO₂ and hard carbon materials for sustainable, cost-effective batteries.

Results and Discussion

Different battery configurations are displayed in Fig. 1. The usage of carbonate electrolytes results in Mn dissolution, migration. and deposition behaviors, which shorten the cycle life of the batteries (Fig. 1a). Carbonate electrolytes also lead to overgrown SEI and significant dendrite formation. An ether electrolyte can potentially enable a MnO₂-based battery with substantially mitigated Mn dissolution (Fig. 1b). However, the use of a complete Li metal anode is still far from being practically feasible. Low-cost carbon anode can be an alternative solution to build a MnO₂-based battery, where a trace amount of Li could be added to compensate the Li loss during cycling (Fig. 1c). Table S1 summarizes the dictating factor of cyclability in different cell configurations. In this study, we gradually build such a rechargeable hard carbon-MnO2 battery cell by identifying individual battery components, investigating their degradation mechanisms and mitigation strategies, and ultimately a full-cell construction. The MnO2||Hard carbon batteries offer a sustainable energy storage solution due to the abundance of raw materials.

We processed commercial EMD with heat treatment to remove water. Figure S1a shows the phase (mostly γ -MnO₂).^{20,21} EMD

consists of micron-sized particles (5-20 μ m) with irregular morphology as displayed in Fig. S1b. Since EMD is a scalable material and has been widely commercialized for primary batteries, we use it as the material to evaluate how different electrolytes perform in the Li metal cells. We first compared the performance of MnO₂ in different electrolytes in Li metal cells (Fig. S2). In general, we found that 1 M LiTFSI DOL/DME (abbreviated as "ether" in the subsequent discussion and figures) can enable the highest capacity retention, whereas 1 M LiPF₆ EC/EMC (abbreviated as "carbonate" in the following figures) causes rapid fading. The 1 M LiTFSI DOL/ DME electrolyte can also provide a slightly increased average discharge voltage. There is a substantially lower buildup of impedance and less Mn dissolution in the 1 M LiTFSI DOL/DME electrolyte. In the ether electrolyte (Figs. 2a-2b), EMD shows an ICE of 69% and a higher reversible capacity of 140 mAh g⁻¹ in the initial cycle at C/3. The capacity retention after 300 cycles at C/3 is as high as $\sim 100\%$. Collectively, our results show that the ether electrolyte is favorable for cycling MnO₂, which provides a great starting point for building the MnO₂llhard carbon full cell.

Next, we investigate how different electrolytes impact the stability of EMD at the surface and in the bulk. To investigate the ensemble-averaged Mn electronic and chemical environments, we analyzed Mn K-edge X-ray absorption near edge structure (XANES) and extended X-ray absorption fine structure (EXAFS). The absorption edge and whiteline shift toward lower energy after discharge, showing Mn reduction (Fig. 3a). At the discharged state, the average Mn oxidation state is 3.28. At the charged state, the average Mn oxidation state is 3.72 (Fig. 3b). We expect that the presence of Mn (III), especially at the end of discharge, can be a source of Mn(III) disproportionation impacted by the electrolyte chemistry. Mn(III) disproportionation forms soluble Mn(II), which is detrimental to the stability of anode interphase and electrolytes. 14 EXAFS probes the local structural environment of Mn (Fig. 3c). The first coordination shell is assigned to Mn-O. We observe a slightly elongated Mn-O corresponding to the Jahn-Teller distorted MnO₆ octahedra in lithiated EMD.²² In the second coordination shell, for pristine MnO₂, a strong peak related to Mn-Mn sharing by edge (Mn-Mn_{edge}) and a weak peak represented by Mn-Mn sharing by corner (Mn-Mn_{corner}) can be found. ^{23,24} Mn₂O₃ gives a very strong Mn-Mn bonding feature, consistent with previous literature. 25 While preserving the Mn-Mn_{edge} and Mn-Mn_{corner} features, the Mn K-edge EXAFS of lithiated EMD is different from that of the pristine sample, suggesting that there are some local structural changes. Despite the abundant Mn(III) and notable change of the Mn coordination environment, EMD delivers negligible capacity decay (Fig. 2), which means the tunnel structure is overall stable during repeated cycling. Such structural integrity might be related to the

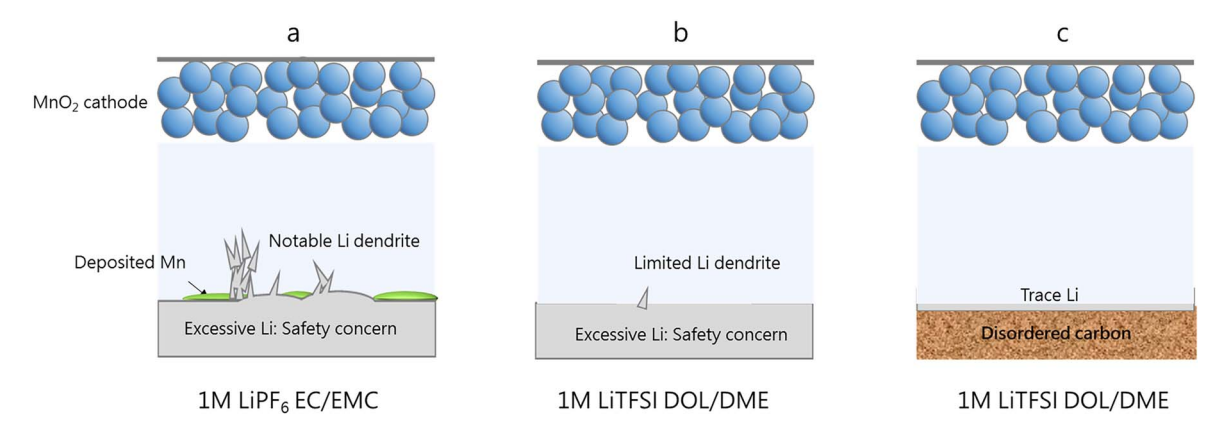


Figure 1. Different configurations of batteries based on a MnO_2 cathode. (a) Li- MnO_2 batteries using carbonate-based electrolytes, exemplified by lithium hexafluorophosphate (LiPF₆) in ethylene carbonate (EC)/ethyl methyl carbonate (EMC) here. EC/EMC = 3/7 by weight. (b) Li- MnO_2 batteries based on ether-based electrolytes, exemplified by 1 M LiTFSI DOL/DME here. DOL/DME = 1/1 by volume. (c) Li/hard carbon- MnO_2 batteries based on 1 M LiTFSI DOL/DME. DOL/DME = 1/1 by volume. A trace amount of Li metal is used to provide Li inventory for cycling and accommodating Li loss, which is in sharp contrast to (a) and (b), where excessive Li metal is used.

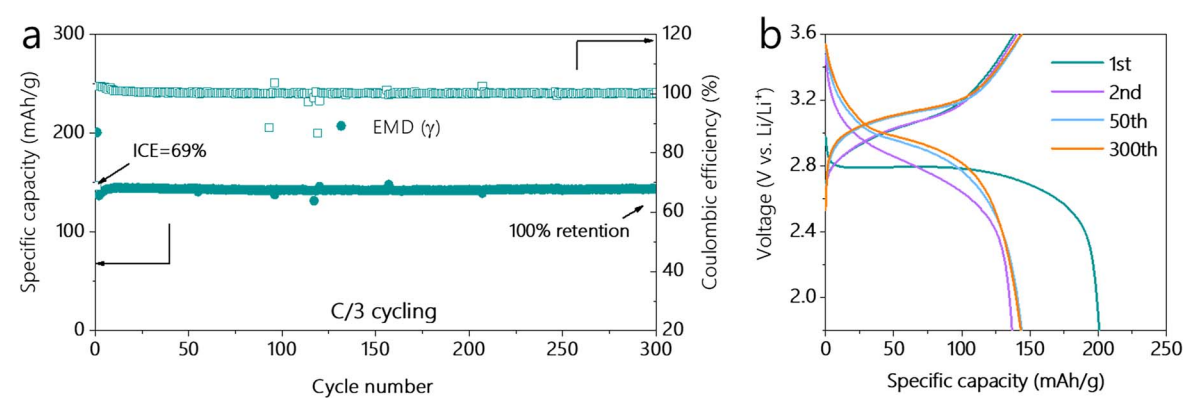


Figure 2. (a) Cycling performance of EMD in 1 M LiTFSI DOL/DME. C/3 is used. $1 \text{ C} = 308 \text{ mAh g}^{-1}$. The voltage range is 1.8 V to 3.6 V. (b) Corresponding voltage profiles of EMD-based cells at a specific cycle number.

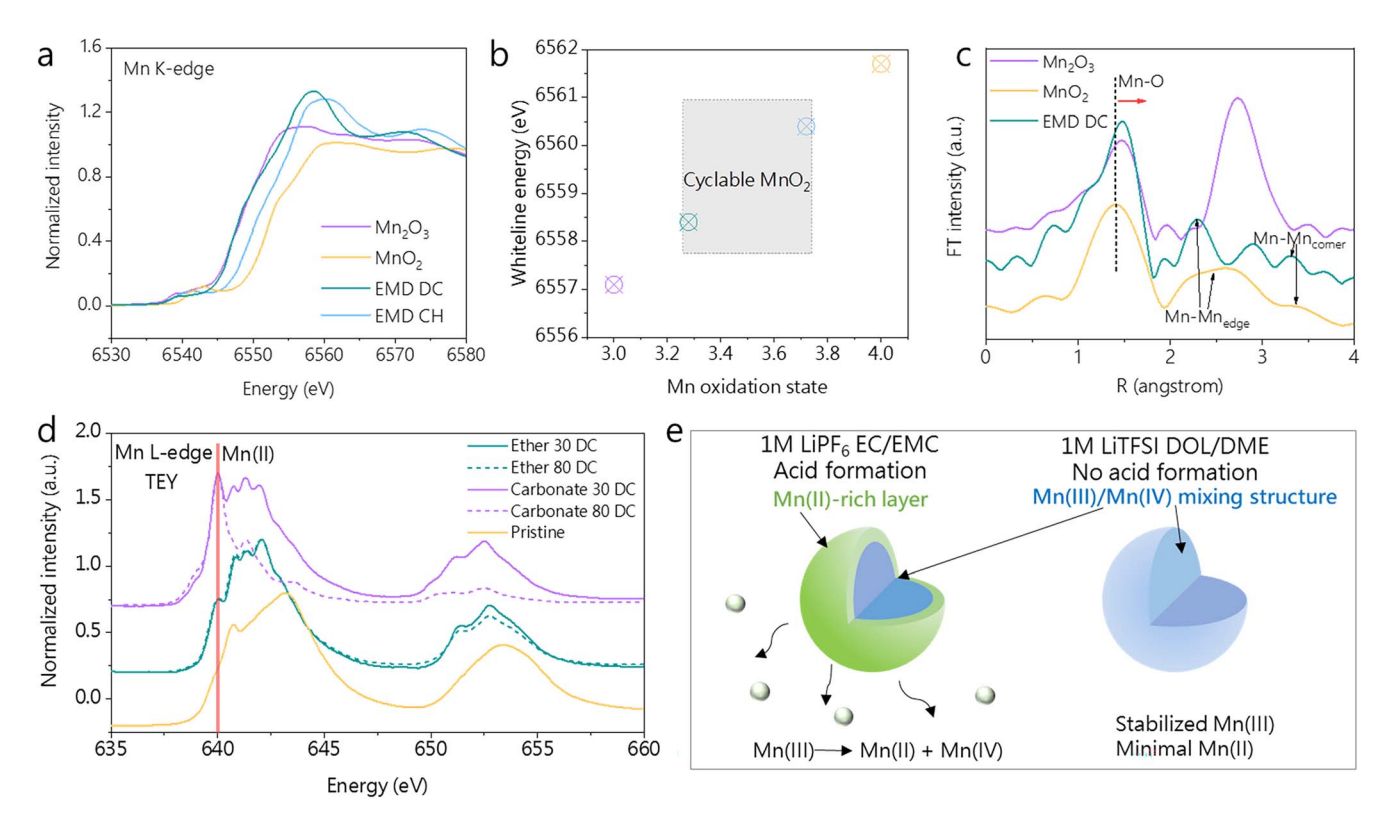


Figure 3. (a) Mn K-edge hard XAS spectra at different states of charge (SOCs). CH means charged to 3.6 V. DC means discharged to 1.8 V. The cycled EMD was collected after fifty cycles at C/3. Mn K-edge XAS spectra of $Mn(IV)O_2$ and $Mn_2(III)O_3$ are provided as references. (b) Calculated Mn oxidation states based on the white-line energy. A linear relationship between oxidation state and energy is assumed. The cyclable Mn oxidation state range is marked. This panel shares the same color scheme as (a). (c) Fourier transformed (FT) magnitude of Mn K-edge EXAFS at different SOCs. (d) Mn L-edge soft XAS spectra of cycled EMD electrodes at different SOCs and in different electrolytes. (e) Schematic of the surface and bulk Mn in EMD after being cycled in carbonate and ether electrolytes.

intergrowth structure, poor crystallinity and defects, which mitigate the Jahn–Teller distortion. 26-28 We then compared the surface Mn states of the electrode after cycling in different electrolytes using soft X-ray absorption spectroscopy (XAS). The pristine MnO₂ exhibits a characteristic of Mn(IV), shown in Figs. 3d and S3a (standard spectra). Cycled in the carbonate electrolyte, the presence of Mn(II) at the surface becomes clear at the 30th cycle and becomes dominant at the 80th cycle. The fluorescence-yield (FY) mode has a probing depth of 50 nm, which means the average thickness of the Mn(II)-rich layer is at least 50 nm (Fig. S3b). Despite the abundance of Mn (III), from the 30th discharge to the 80th discharge, the surface chemical state of Li_xMnO₂ cycled in the ether electrolyte has an insignificant change. At the 80th discharge, there is no major difference in XRD (Fig. S4). In Fig. 3e, the schematic depicts the

surface evolution of $\mathrm{Li_xMnO_2}$ in the ether and carbonate electrolytes. The carbonate electrolytes produce HF via the $\mathrm{PF_6}^-$ hydrolysis, boosting the disproportionation reaction of Mn(III) and the formation of soluble Mn(II). ¹³ In contrast, with the ether electrolyte utilizing lithium imide salts resilient to hydrolysis, the Mn(III) disproportionation is mitigated. ¹⁶ Collectively, we show that Mn-based materials are stabilized in the ether electrolyte, which would help the MnO₂||hard carbon full cell.

Despite the excellent rechargeability of MnO₂ cathodes, a suitable anode is needed for large-scale energy storage because cost and safety are particularly critical over energy density. Ether electrolytes generally have poor compatibility with the commercial graphite anode, and thus no full-cell design has been reported to the best of our knowledge. ¹⁸ Here, we study the compatibility of the 1 M LiTFSI

DOL/DME electrolyte with a hard carbon anode. It is well known that in Na and K chemistries, hard carbon can exhibit higher capacity, faster charge capability, and outstanding cycling life in ether-based electrolytes over carbonate-based electrolytes. We wonder if the trend can be replicated in LIBs. According to the cyclic voltammetry (CV) data (Fig. 4a), the electrolyte undergoes reduction during the first discharge, suggesting a noticeable SEI formation. The curves overlap well beyond the second cycle, suggesting the excellent reversibility of the electrochemical cell. In Figs. 4b-4c, the rate capability test at different current densities (from 0.1 A g 1 A g⁻¹) demonstrates that hard carbon delivers a high CE (>99.5%) and a decent capacity at high current density, for example, 120 mAh g⁻¹ at 1 A g⁻¹. The sloping voltage profile indicates an adsorptionbased reaction mechanism. In addition, the average discharge voltage is much higher than the Li metal plating potential, which is beneficial to fast-charging and low-temperature operations. The specific capacity of hard carbon cycled in the ether electrolyte is higher than that cycled in the carbonate electrolyte (Figs. 4d-4f). Both electrolytes provide similar coulombic efficiencies, with an ICE (\sim 75%) and an average CE (>99.5%). After 250 cycles, the capacity retention is \sim 86%. To conclude, the ether electrolyte performs better than the carbonate electrolyte. In addition, no plateau capacity is observed cycled in the 1 M LiTFSI DOL/DME electrolyte. The origin of plateau-capacity in hard carbon anode remains controversial. Several mechanisms have been proposed, including pore filling, Na-ion insertion, and cation-solvent co-intercalation. Our results indicate that the reaction mechanism of hard carbon in the DOL/DME electrolyte is predominantly surface adsorption (Fig. 4g). When paired with a MnO₂ cathode, a MnO₂||hard carbon full cell performs intercalation and adsorption reaction mechanisms in the cathode and anode, respectively.

At this point, the compatibility of hard carbon and MnO_2 with the ether electrolyte has been substantiated. Both electrodes are Li-free in the as-synthesized state. Therefore, we need limited Li metal as a Li-ion source for the Li-free electrodes. Thus, a thin Li metal foil is pressed with hard carbon, akin to a pre-lithiation process. Figure 4h shows that after 24 h the open circuit voltage (OCV) of the cell can reach ~ 0 V vs Li/Li⁺, suggesting successful "contact pre-lithiation."

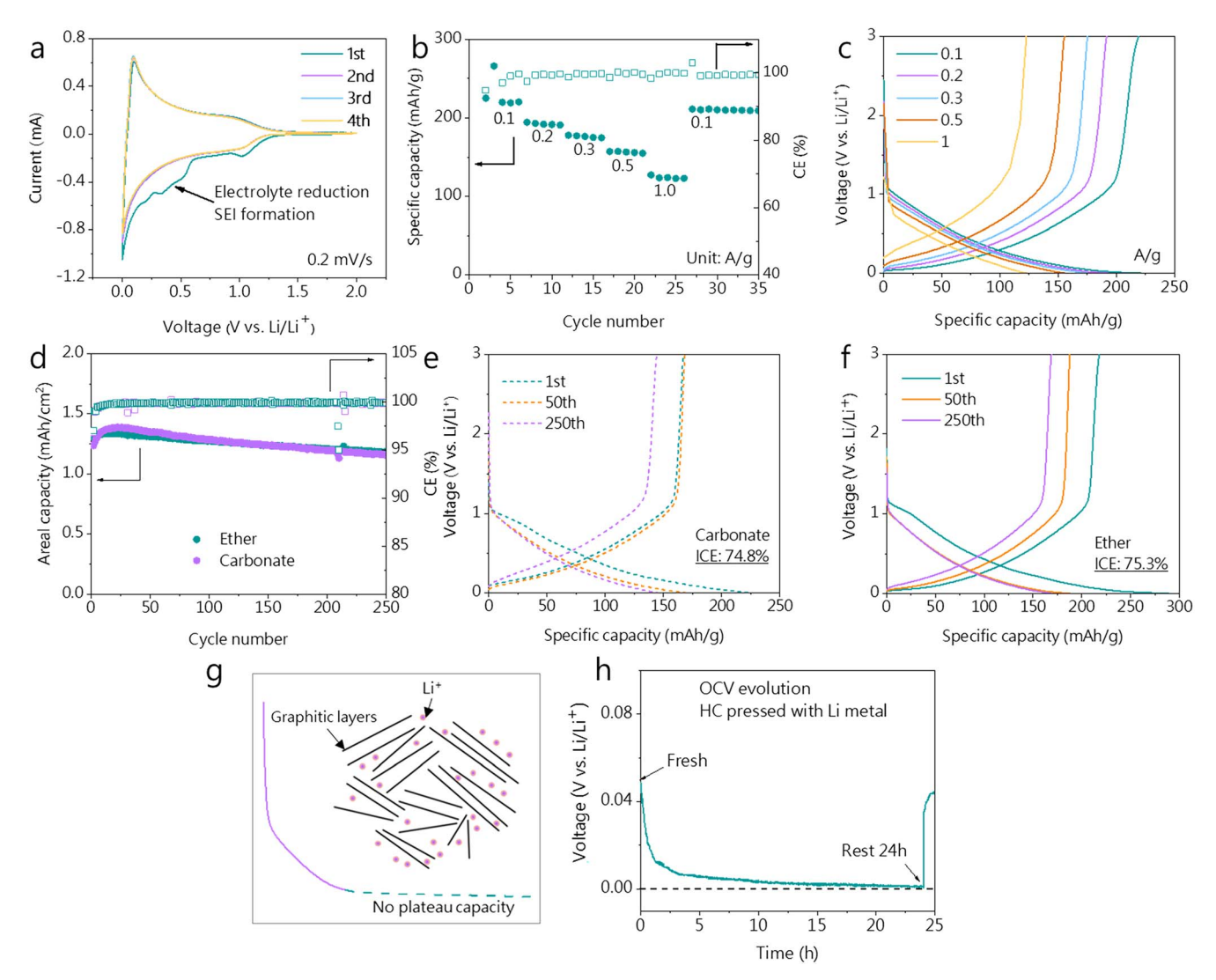


Figure 4. (a) Cyclic voltammetry plots of hard carbonllLi metal cells in 1 M LiTFSI DOL/DME at 0.2 mV s⁻¹. (b) Rate capability of hard carbon in the ether electrolyte at different current densities. (c) Corresponding voltage profiles of (b). (d) Cycling performances of hard carbonllLi metal cells in 1 M LiTFSI DOL/DME and 1 M LiPF₆ EC/EMC at 0.1 A g⁻¹. The mass loading of hard carbon cycling in 1 M LiTFSI DOL/DME and 1 M LiPF₆ EC/EMC is 7.0 mg cm⁻² and 8.0 mg cm⁻², respectively. (e)-(f) Voltage profiles of hard carbon in different electrolytes at a specific cycle number. (g) Schematic of the proposed Li-ion storage mechanism in hard carbon. The curve is modified from real data of the hard carbon in Na-ion batteries. (h) The evolution of the open circuit voltage (OCV) of a hard carbon/Li composite electrode in 1 M LiTFSI DOL/DME. A small piece of Li metal (4 mm diameter) is directly pressed on the center of a hard carbon anode (10 mm diameter). The mass of Li metal is 2.0 mg while the mass of hard carbon is 6.2 mg. The composite electrode then follows the conventional cell assembly process using a Li metal disk as the counter electrode. The changing OCV indicates the successful prelithiation of hard carbon by the Li metal.

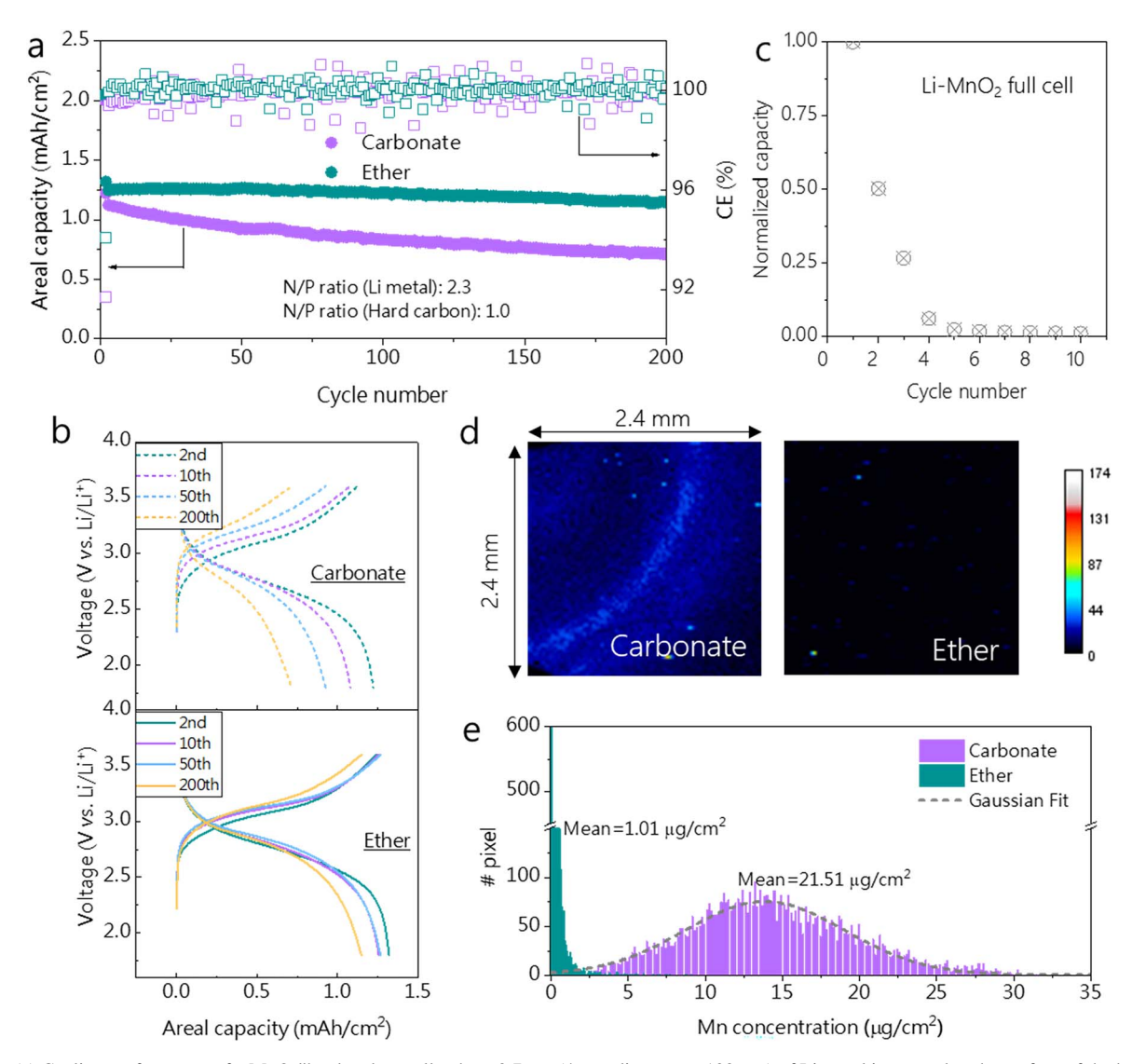


Figure 5. (a) Cycling performance of a MnO₂llhard carbon cell, where 0.7 mg (4 mm diameter, ~100 μ m) of Li metal is pressed to the surface of the hard carbon anode. In the N/P ratio calculation, 220 mAh g⁻¹ and 3860 mAh g⁻¹ are used for hard carbon and Li metal, respectively. 130 mAh g⁻¹ is used for MnO₂. Mass loading of MnO₂: 12 mg cm⁻². Carbonate and ether electrolytes are used. C/20 is used in the formation cycle and C/5 is applied in the following cycles. A voltage window from 1.8 V to 3.6 V is used. (b) The corresponding voltage profiles of full cells in (a) at specific cycle numbers. (c) Cycling performance of Li-MnO₂ batteries with limited Li metal. The N/P ratio is around 2.6. The first discharge capacity is used for normalization. (d) Fluorescence X-ray mapping of the cycled hard carbon electrode. The X-axis and Y-axis contain 80 pixels each, and one pixel is 30 μ m*30 μ m in area. The scale bar has a unit of μ g/cm². (e) The corresponding Mn elemental distribution histogram calculated from maps in (d). The R-square of the Gaussian fitting is 0.96.

Figure 5a presents the cycling performance MnO₂llhard carbon full cells, where the hard carbon anode surface has a small piece of Li metal $(0.7 \text{ mg}, 4 \text{ mm diameter}, \sim 100 \,\mu\text{m})$. Note that the full cell here is only a proof of concept. The usage of Li metal can be further reduced. During the early cycles, Li metal provides Li inventory and compensates for the Li loss due to the SEI formation on the hard carbon anode and irreversible Li intercalation in the cathode. The cells deliver a similar initial areal capacity of 1.26 mAh cm⁻² in the two electrolytes. After 200 cycles, the capacity retention in the ether electrolyte is 91%, which is much higher than that in the carbonate electrolyte (58%) (Fig. 5a). The voltage profile (Fig. 5b) shows that the cell cycled in the carbonate electrolyte has a rapid decrease of energy density and energy efficiency. Our results further show the high compatibility between the ether electrolyte and hard carbon and MnO₂ electrodes. When the small piece of Li metal is used as the stand-alone anode (Fig. 5c), the capacity of the Li-MnO₂ cell drops to <5% after five cycles. In addition, the cell has a low ICE of 70%, similar to that of Li-MnO₂ battery with excessive Li metal (Fig. 2b). These results demonstrate that hard carbon is indeed the main electrochemically active component in the MnO₂||hard carbon full cell.

To quantify Mn deposited on the hard carbon, fluorescence X-ray mapping was performed on the surface of the hard carbon anode after 200 cycles in the two electrolytes (Figs. 5d–5e). Only a few spots with high Mn intensities are observed in the ether electrolyte. In contrast, noticeable Mn deposition can be observed in the carbonate electrolyte (the mean Mn concentration is $21.51~\mu g~cm^{-2}$). The concentration of the deposited Mn follows a normal distribution or Gaussian distribution.

Conclusions

In this work, we provide a comprehensive study of manganese oxide and hard carbon in half and full cells. MnO_2 is shown to be intrinsically reversible in Li-ion storage. The electrolyte is the key to mitigating Mn dissolution and maximizing the cycle life of EMD. In the ether electrolyte (1 M LiTFSI DOL/DME), a capacity retention of $\sim 100\%$ is achieved after 300 cycles at C/3, outperforming the 1 M LiClO₄ PC/DME and 1 M LiPF₆ EC/EMC electrolytes. Supported by synchrotron X-ray spectroscopic data, the Mn(II)-rich layer originated from the disproportionation mechanism is

minimized by using the ether electrolyte. We also demonstrate the compatibility between the hard carbon anode and the ether electrolyte. The adsorption-based mechanism provides a capacity of $\sim\!\!230$ mAh g $^{-1}$. Based on these findings, we fabricate MnO₂llhard carbon full cells with a lean Li metal to provide the initial Li inventory and accommodate the low ICE of hard carbon. Cycling in the ether electrolyte offers a higher cycling performance and substantially mitigates Mn dissolution. In summary, the utilization of Earthabundant, low-cost, and scalable manganese oxides and hard carbon show promises for energy storage systems.

Materials Preparation and Cell Fabrication

Commercial electrolytic manganese dioxide (EMD) was purchased from Thermo Scientific Chemicals (activated, tech. 90%,). The material was then heated at 350 °C in the air for 12 h. The electrode slurry is composed of 90 wt% heated EMD, 5 wt% carbon black, and 5 wt% polyvinylidene fluoride (PVDF), homogenously dispersed in N-methyl-2-pyrrolidinone (NMP). The slurry is cast onto aluminum foils first dried at 80 °C for 4 h and then at 120 °C for overnight in a vacuum oven. Commercial hard carbon is ordered from MSE Supplies LLC. The electrode slurry is composed of 90 wt% hard carbon, 2.5 wt% carbon black, and 7.5 wt% sodium alginate, homogenously dispersed in deionized (DI) water. The slurry is cast onto aluminum foils first dried at 80 °C for 4 h and then at 120 °C for overnight in a vacuum oven. Electrodes are cut into discs of 10 mm diameter. The average mass loading of the cathode electrode for halfcell configuration was 3.0-4.0 mg cm⁻². The 2032-coin cells are assembled in an Argon filled glovebox. Half cells were made with manganese dioxide as the working electrode. Li metal as the counter electrode, and Celgard 2325 as the separator. Flooded electrolytes are used in each cell. In full cell preparation, thin Li metal (4 mm diameter) is manually rolled and pressed on the top of hard carbon.

Electrochemical Measurements

The constant-current charge/discharge tests were performed on the Land battery-testing system. All batteries were cycled at room temperature (22 °C–23 °C). The voltage range of cathode measurement is 1.8 to 3.6 V vs Li/Li⁺. The specific capacity shown in the software is divided by 0.9 since the purity of EMD is 90%. The voltage range of hard carbon anode measurement is 0.001 to 3.0 V vs Li/Li⁺. The voltage range of the MnO₂llhard carbon full cell is 1.8 to 3.6 V. Electrochemical impedance spectroscopy (EIS) was tested on an electrochemical potentiostat (Princeton Versa STAT3) with a frequency range of 100k-0.01 Hz and a potential amplitude of 5 mV s⁻¹. Cyclic voltammetry (CV) was conducted on the same potentiostat.

Material Characterizations

The scanning electron microscopy (SEM)-energy dispersive spectroscopy (EDS) mapping was performed on a scanning electron microscope (FESEM, LEO 1550). X-ray diffraction (XRD) data was measured on a Bruker D8 Advance diffractometer with Cu Klphasource. The cycled electrode was fixed and covered with Kapton tape. Soft X-ray adsorption spectroscopy (soft XAS) was obtained at Beamline 10-1 in Stanford Synchrotron Radiation Lightsource (SSRL). Data were acquired under ultrahigh vacuum (10^{-9} Torr) at room temperature. The energy resolution is approximately 0.2 eV, and the beam spot measures about 1 mm². Samples were affixed to an Aluminum sample holder within an argon-filled glovebox and securely sealed during transfer. The soft XAS data was analyzed by Pymca. Normalization to [0,1] was applied for the collected data. The energy correction was conducted based on the reference spectra and the characteristic peak of Mn (II) at 640 eV. Hard X-ray adsorption spectroscopy (hard XAS) was conducted at beamline 20-BM in the Advanced Photon Source at Argonne National Laboratory. The electrode underwent a sealing process with Kapton tape before measurements. Analysis of XANES and

EXAFS data was performed using ATHENA software following standard methods. The X-ray fluorescence microscopy (XFM) data were gathered at the 8-BM beamline at the Advanced Photon Source, Argonne National Laboratory, utilizing a sub-micrometer focused 10-keV X-ray beam with a step size of 30 μ m, while the samples were raster-scanned. The hard carbon was peeled off from the Cu current collector prior to the XFM measurements to avoid interference signal from Cu. XFM data was analyzed by ImageJ. For all the electrodes used in synchrotron experiments, dimethyl carbonate (DMC) solvent was employed to remove the residual salts.

Acknowledgments

The work was supported by the Sun Grant program of the National Institute of Food and Agriculture (NIFA), USDA, USA. The synchrotron methods used to perform the characterization work were partially supported by and developed under the National Science Foundation (No. DMR-2045570). This work used shared facilities at the Nanoscale Characterization and Fabrication Laboratory, which is funded and managed by Virginia Tech's Institute for Critical Technology and Applied Science. Additional support is provided by the Virginia Tech National Center for Earth and Environmental Nanotechnology Infrastructure (NanoEarth), a member of the National Nanotechnology Coordinated Infrastructure (NNCI), supported by NSF (ECCS 1542100 and ECCS 2025151).

ORCID

Dawei Xia https://orcid.org/0000-0003-4265-2528 Feng Lin https://orcid.org/0000-0002-3729-3148

References

- M. S. Whittingham, "Lithium batteries: 50 years of advances to address the next 20 years of climate issues." Nano Lett., 20, 8435 (2020).
- E. A. Olivetti, G. Ceder, G. G. Gaustad, and X. Fu, "Lithium-ion battery supply chain considerations: analysis of potential bottlenecks in critical metals." *Joule*, 1, 229 (2017)
- B. E. Murdock, K. E. Toghill, and N. Tapia-Ruiz, "A perspective on the sustainability of cathode materials used in lithium-ion batteries." Adv. Energy Mater., 11, 2102028 (2021).
- K. Turcheniuk, D. Bondarev, V. Singhal, and G. Yushin, "Ten years left to redesign lithium-ion batteries." *Nature*, 559, 467 (2018).
- Y. Huang, Y. Dong, S. Li, J. Lee, C. Wang, Z. Zhu, W. Xue, Y. Li, and J. Li, "Lithium manganese spinel cathodes for lithium-ion batteries." *Adv. Energy Mater.*, 11, 2000997 (2021).
- J. Shin, J. K. Seo, R. Yaylian, A. Huang, and Y. S. Meng, "A review on mechanistic understanding of MnO2 in aqueous electrolyte for electrical energy storage systems." *Int. Mater. Rev.*, 65, 356 (2020).
- Y. Hu, T. Zhang, F. Cheng, Q. Zhao, X. Han, and J. Chen, "Recycling application of Li–MnO2 batteries as rechargeable lithium-air batteries." *Angew. Chem. Int. Ed.*, 54, 4338 (2015).
- K. He, Y. Yuan, W. Yao, K. You, M. Dahbi, J. Alami, K. Amine, R. Shahbazian-Yassar, and J. Lu, "Atomistic insights of irreversible Li+ intercalation in MnO2 electrode." *Angewandte Chemie International Edition*, 134, 2 e202113420 (2022).
 Y. Yuan et al., "Ordering heterogeneity of [MnO6] octahedra in tunnel-structured
- 9. Y. Yuan et al., "Ordering heterogeneity of [MnO6] octahedra in tunnel-structured MnO2 and its influence on ion storage." *Joule*, **3**, 471 (2019).
- W.-M. Chen, L. Qie, Q.-G. Shao, L.-X. Yuan, W.-X. Zhang, and Y.-H. Huang, "Controllable synthesis of hollow bipyramid β-MnO2 and its high electrochemical performance for lithium storage." ACS Appl. Mater. Interfaces, 4, 3047 (2012).
- performance for lithium storage." ACS Appl. Mater. Interfaces, 4, 3047 (2012).
 11. J.-Y. Luo, J.-J. Zhang, and Y.-Y. Xia, "Highly electrochemical reaction of lithium in the ordered mesoporosus β-MnO2." Chem. Mater., 18, 5618 (2006).
- E. Moazzen, K. Kucuk, S. Aryal, E. V. Timofeeva, and C. U. Segre, "Nanoscale MnO2 cathodes for Li-ion batteries: effect of thermal and mechanical processing." *J. Power Sources*, 448, 227374 (2020).
- C. Zhan, T. Wu, J. Lu, and K. Amine, "Dissolution, migration, and deposition of transition metal ions in Li-ion batteries exemplified by Mn-based cathodes—a critical review." *Energy Environ. Sci.*, 11, 243 (2018).
 Y. Zhang, A. Hu, D. Xia, S. Hwang, S. Sainio, D. Nordlund, F. M. Michel, R.
- Y. Zhang, A. Hu, D. Xia, S. Hwang, S. Sainio, D. Nordlund, F. M. Michel, R. B. Moore, L. Li, and F. Lin, "Operando characterization and regulation of metal dissolution and redeposition dynamics near battery electrode surface." *Nat. Nanotechnol.*, 18, 790–797 (2023).
- H. Y. Asl and A. Manthiram, "Reining in dissolved transition-metal ions." Science, 369, 140 (2020).
- D. Xia, H. Gao, M. Li, J. Holoubek, Q. Yan, Y. Yin, P. Xu, and Z. Chen, "Enabling rechargeable Li-MnO2 batteries using ether electrolytes." SmartMat, 4, e1208 (2023).
- D. Hou, D. Xia, E. Gabriel, J. A. Russell, K. Graff, Y. Ren, C.-J. Sun, F. Lin, Y. Liu, and H. Xiong, "Spatial and temporal analysis of sodium-ion batteries." ACS Energy Lett., 6, 4023 (2021).

- 18. D. Xia et al., "Design criteria of dilute ether electrolytes toward reversible and fast intercalation chemistry of graphite anode in li-ion batteries." ACS Energy Lett., 8, 1379 (2023).
- Y. Li, F. Wu, Y. Li, M. Liu, X. Feng, Y. Bai, and C. Wu, "Ether-based electrolytes 19 for sodium ion batteries." Chem. Soc. Rev., 51, 4484 (2022).
- 20. J.-R. Hill, C. M. Freeman, and M. H. Rossouw, "Understanding γ -MnO2 by
- molecular modeling." *J. Solid State Chem.*, 177, 165 (2004).
 21. M. R. Bailey and S. W. Donne, "Structural effects on the cyclability of the alkaline γ-MnO2 electrode." *Electrochim. Acta*, 56, 5037 (2011).
- 22. M. M. Rahman et al., "Chemical modulation of local transition metal environment enables reversible oxygen redox in Mn-Based layered cathodes." ACS Energy Lett., 6, 2882 (2021).
- 23. S. Kong, A. Li, J. Long, K. Adachi, D. Hashizume, Q. Jiang, K. Fushimi, H. Ooka, J. Xiao, and R. Nakamura, "Acid-stable manganese oxides for proton exchange membrane water electrolysis." *Nat. Catal.* (2024).
- 24. H. Jiang et al., "An aqueous dual-ion battery cathode of Mn3O4 via reversible insertion of nitrate." *Angew. Chem. Int. Ed.*, **58**, 5286 (2019).

 25. S. Tsunekawa, F. Yamamoto, K.-H. Wang, M. Nagasaka, H. Yuzawa,
- S. Takakusagi, H. Kondoh, K. Asakura, T. Kawai, and M. Yoshida, "Operando

- observations of a manganese oxide electrocatalyst for water oxidation using hard/ tender/soft X-ray absorption spectroscopy." J. Phys. Chem. C, 124, 23611 (2020).
- 26. R. R. Maphanga, D. C. Sayle, T. X. Sayle, and P. E. Ngoepe, "Amorphization and recrystallization study of lithium insertion into manganese dioxide." Phys. Chem. Chem. Phys., 13, 1307 (2011).
- 27. N. P. L. Magnard, A. S. Anker, O. Aalling-Frederiksen, A. Kirsch, and K. M. Ø. Jensen, "Characterisation of intergrowth in metal oxide materials using structuremining: the case of γ -MnO2." *Dalton Trans.*, **51**, 17150 (2022).
- X. Zhu et al., "LiMnO2 cathode stabilized by interfacial orbital ordering for sustainable lithium-ion batteries." Nature Sustainability, 4, 392 (2021).
- 29. L. Tao, P. Sittisomwong, B. Ma, A. Hu, D. Xia, S. Hwang, H. Huang, P. Bai, and F. Lin, "Tailoring solid-electrolyte interphase and solvation structure for subzero temperature, fast-charging, and long-cycle-life sodium-ion batteries." Energy Storage Mater., 55, 826 (2023).
- 30. M. Ma, H. Cai, C. Xu, R. Huang, S. Wang, H. Pan, and Y.-S. Hu, "Engineering solid electrolyte interface at nano-scale for high-performance hard carbon in sodium-ion batteries." Adv. Funct. Mater., 31, 2100278 (2021).
- 31. B. Ravel and M. Newville, "ATHENA, ARTEMIS, HEPHAESTUS: data analysis for X-ray absorption spectroscopy using IFEFFIT." J. Synchrotron Radiat., 12, 537 (2005).